CARBON 64 (2013) 527–536

Available at www.sciencedirect.com

ScienceDirect

journal homepage: www.elsevier.com/locate/carbon

Microwave self-assembly of 3D graphene-carbon nanotube-nickel nanostructure for high capacity anode material in lithium ion battery

Seok-Hu Bae [a], Kaliyappan Karthikeyan [b], Yun-Sung Lee [b,*], Il-Kwon Oh [a,*]

[a] Graphene Research Center, KAIST Institute for the NanoCentury, School of Mechanical, Aerospace and Systems Engineering, Division of Ocean Systems Engineering, Korea Advanced Institute of Science and Technology, 335 Gwahak-ro, Yuseong-gu, Daejeon 305-701, Republic of Korea

[b] Faculty of Applied Chemical Engineering, Chonnam National University, Gwang-ju 500-757, Republic of Korea

ARTICLE INFO

Article history:
Received 13 May 2013
Accepted 3 August 2013
Available online 9 August 2013

ABSTRACT

We report a microwave-assisted synthesis of a self-assembled three-dimensional graphene-carbon nanotube-nickel (3D G-CNT-Ni) nanostructure, which can be used as a high capacity anode material in lithium-ion batteries (LIBs). The unique 3D G-CNT-Ni nanostructure shows that CNTs are grown on graphene sheets through tip growth mechanism by Ni nano-particles. Bunches of CNTs and graphene sheets produce 3D network nanostructures with ultrahigh surface area, a large number of activation sites, and efficient ion pathways, all of which are crucial for high capacity anode materials in LIBs. The synthesized 3D nanostructure maintains a reversible specific capacity of 648.2 mA h/g after 50 cycles at a current density of 100 mA/g, as high capacity electrode structures in LIBs.

1. Introduction

As an energy storage system, rechargeable lithium-ion batteries (LIBs) have been applied to various mobile systems such as mobile phones, portable electronics, electric vehicles, plug-in hybrid electric vehicles, and hybrid electric vehicles. As the consumption of electric power greatly increases, significant improvements in the performance indexes of LIBs are impending such as rate capability, cycle life, energy density, and power density. As an anode material, graphene, has recently come to be considered as a highly potential substitute material for commercial graphite which has a theoretical specific capacity of 372 mA h/g [1,2]. Compared to graphite, graphene can exhibit much higher capacities owing to its larger number of exposed edges, larger surface area, high conductivity, structural defects, chemical stability and extra space for lithium-ion storage. However, experimental results on graphene used as an anode material show poor reversible capacity and poor cycle life because of structural limits such as re-stacking nature [1–5].

Hence, considerable efforts have been made to overcome the structural limits of graphene. One new avenue is to integrate carbon-based nanostructures into a hybrid material in order to obtain synergy effect [6–17]. With the use of graphene, some morphologically modified carbon nanostructures such as carbon nanotubes (CNTs), fullerenes, activated carbon, and carbon aerogels have been reported [6–8]. Especially three-dimensional (3D) carbon nanostructures obtained by combining two-dimensional planar graphene with one-dimensional vertical CNTs have attracted much interest because of their structural merits [9,10,12,15]. The geometric form of 3D carbon nanostructures aligns the conductivity paths in the planar direction with graphene and in the axial direction with CNTs, leading to minimal resistance. Additionally if CNTs are directly bonded to the graphene, it is possible to minimize the contact resistance at junction

* *Corresponding authors:* Fax: +82 42 350 1520 (I.-K. Oh), +82 62 530 1909 (Y.-S. Lee).
E-mail addresses: leeys@chonnam.ac.kr (Y.-S. Lee), ikoh@kaist.ac.kr (I.-K. Oh).
0008-6223/$ - see front matter
http://dx.doi.org/10.1016/j.carbon.2013.08.003

[18–19]. Lowering of resistance directly contributes to increasing the current access on the anode, enhancing the diffusion of Li-ion toward the electrode. Additionally, the resulting 3D carbon nanostructures possess high surface-to-volume ratio, which is a key parameter in LIBs in terms of both high capacity and energy density. In addition, the bundling of graphene is overcome by the CNTs as role of spacer in their structures. As a result, this structural system can be directly applied as performance enhancers in LIBs. Previously, 3D carbon nanostructures were usually prepared by chemical vapor deposition [9–12], plasma-enhanced chemical vapor deposition [13], chemical reduction with hydrazine [14], etc. However, some synthetic methods involve multiple steps and processing difficulties due to the use of high temperature conditions and expensive apparatus in addition to the time-consuming and hazardous nature of such processes. Therefore, a one-pot, cost-effective, and simple self-assembly method to form 3D carbon nanostructures remains a challenging topic and is indispensable to the energy storage community.

Meanwhile, several studies have attempted to use composite materials of graphene and CNTs as anode materials in LIBs. Yoo et al. reported the preparation of CNT and graphene nanostructures using acid-treatment followed by ultrasonic mixing; these materials utilized as anode materials and demonstrated a reversible capacity of 480 mA h/g after 20 cycles at a current density of 50 mA h/g [6]. Chen et al. demonstrated the hybridization of CNT-graphene through in situ chemical vapor deposition process; these materials exhibited a reversible capacity of 518 mA h/g after 30 cycles at a current density of 74 mA h/g [15]. Fan et al. prepared composites of carbon nanofibers (CNFs) grown on graphene through chemical vapor deposition approach; these materials had a reversible capacity of 607 mA h/g after 30 cycles at a current density of 0.12 mA/cm^2 [12]. Recently, Sun et al. successfully fabricated reduced graphene oxide-CNT composites using microwave-assisted synthesis by adjusting the weight percentage of CNTs [16,17]. Even though graphene and CNT composites show synergetic effects in terms of electrochemical activity, it is difficult to keep the specific capacity stable from the early stages of cycles. As a result, graphene and CNT composites delivered a reversible capacity of 298 mA h/g after 50 cycles at a current density of 50 mA/g. In short, the poor electrochemical performances may result from the absence of direct bonding between graphene and CNTs because the researchers used commercial CNTs that were not directly grown on the surface of the graphene sheets. The direct bonded conjunction between the graphene and the CNTs significantly contributes to not only maintaining a stable level of work function in carbon structures but also giving rise to efficient charge transfer and Li-ion migration, thereby enhancing the Li-ion storage properties [20].

Herein, we report a cost-effective microwave self-assembly of a 3D graphene-carbon nanotube-nickel (G-CNT-Ni) nanostructure composed of graphene sheets and CNTs. To the best of our knowledge, nickel nano-particles have not yet been used to construct 3D carbon nanostructures or their derivatives for adoption as anode materials for LIBs. These novel 3D G-CNT-Ni functional nanostructures show excellent performance in terms of their high lithium storage capacity with improved reversible cycling stability; they also have high rate capacity due to their high surface area, high porosity, and non-stacking of graphene layers.

2. Experimental

2.1. *Preparation of self-assembled 3D nanostructure*

The self-assembled 3D G-CNT-Ni nanostructure has been synthesized in a two-step process. In the first step, expandable graphite oxide was prepared using the modified Hummer's method [21]. And expandable graphite oxide powder was added to 200 mL of deionized water, followed by ultrasonication for 30 min. The above solution was filtered and dried in a vacuum oven. This dried material was added to an empty 500 ml beaker, which was covered with wiper. And then the beaker was put on the hot plate at 400 °C for 5 min. The resulting fluffy-black powder is called thermally exfoliated reduced graphene oxide (TErGO). In the second step, the TErGO powder was mixed with an appropriate amount of nickelocene ($Ni(C_5H_5)_2$) and was dispersed in acetonitrile (CH_3CN), followed by ultrasonication for 30 min. Finally, the above mixture was placed in a microwave oven (MAS-II, SSMCT Co. Ltd., China) and was irradiated at 700 W for 5 min, then the microwave was turned off and the mixture was allowed to cool for 5 min. After that, the mixture was irradiated at 700 W for 5 min again. Finally the 3D G-CNT-Ni nanostructure was synthesized through the above two-step process. Bamboo CNTs which are a reference sample for comparison were synthesized within the second step, excluding TErGO.

2.2. *Characterization*

The physical characterization of self-assembled 3D nanostructures was examined using X-ray diffractometry (XRD, D/MAX-2500, Japan), field emission scanning electron microscopy (FESEM, Magellan-400, Nova230, Japan), transmission electron microscopy (FETEM, Tecnai F20, USA), high resolution dispersive Raman spectroscopy (LabRAM HR UV/Vis/NIR, France), Fourier transform infrared spectroscopy (FT-IR, 4100 Jasco, Japan), multipurpose X-ray photoelectron spectroscopy (XPS, Sigma Probe, UK), Brunauer Emmett Teller (BET, Tristar ll 3020 V1.03, Micromeritics, USA) surface area characterization and thermogravimetric analysis (TGA, 92-18, Setaram, France). The electrochemical measurements were performed using a CR2032 coin cell configuration in which the synthesized nanostructures were used as the working electrode and lithium foil acted as the counter electrode. The composite anodes were prepared by pressing a slurry containing 5 mg of 3D G-CNT-Ni nanostructures or bamboo CNT active materials, 1 mg of Ketzen black (KB), and 1 mg of teflonized acetylene black on a 200 mm^2 nickel mesh; this mixture was dried at 160 °C for 4 h in a vacuum oven. The test cells were fabricated in an argon filled glove box by pressing of the prepared anodes along with a lithium foil cathode separated by a polypropylene separator (Celgard 2600, USA). 1 M $LiPF_6$ (1:1 v/v EC:DMC, Soulbrain, Korea) was used as the electrolyte. All electrochemical tests were performed using the constant current method. Electrochemical profiles were obtained in the voltage range of 0–3 V at a

current density of 100 mA/g using a battery tester system (PNE solution, Korea). The electrochemical impedance spectroscopy (EIS, BIO-LOGIC, SP-150, France) measurements were carried out in the frequency range of 0.1 Hz to 100 kHz.

3. Results and discussion

A schematic representation of the formation process of the self-assembled 3D G-CNT-Ni nanostructure and its role as an anode material in LIB is given in Fig. 1. During the ultrasonication process, nickelocene ($Ni(C_5H_5)_2$) and acetonitrile (CH_3CN) dispersed between and on the graphene sheets. When the mixture was subjected to microwave irradiation, the $Ni(C_5H_5)_2$ organometallics thermally decomposed into nickel nanoparticles and hydrocarbon molecules; theses nickel nanoparticles induce the growth of CNTs, as shown in Fig. 1. Importantly, carbonaceous gases that arose from acetonitrile were captured by the nickel nanoparticles, forming carbon-coated nickel nanoparticles [22]. The graphene defects acted as nucleation sites and anchoring sites for the nickel nanoparticles; then, the nickel nanoparticles release the dissolved carbon, leading to CNT growth. This CNT growth follows the 'tip-growth' mechanism [23]. Additionally, it is well known that decomposed nitrogen from CH_3CN contributes to the formation of bamboo-shaped CNT structures with atomic defects.

The surface morphology of the self-assembled 3D G-CNT-Ni nanostructures was characterized by FE-SEM. Fig. 2 shows the SEM images of the thermally exfoliated graphene precursor, the nickel-decorated graphene sheets, and the 3D G-CNT-Ni nanostructures. Fig. 2a shows the rippled and fluffy nature of the thermally-exfoliated graphene sheets [24], which were used as the starting material for the synthesis of the 3D G-CNT-Ni nanostructures. Some scrolling of the graphene sheet was caused by thermal exfoliation during the reduction process [24]. In the middle of microwave irradiation to the homogenous mixture, we found that nickel nanoparticles were uniformly decorated on the graphene sheets, as shown in Fig. 2b. The bright and white dots on the graphene sheets represent the nickel nanoparticles. During the CNT growth, nickel nanoparticles mainly adhered to the surface of the graphene sheet or between the graphene sheets.

These nickel nanoparticles were encapsulated inside CNTs in the initial stages [25], which led to upward growth of CNTs from the graphene root. Fig. 2c shows the initial growth of CNTs on the graphene sheets after short-time microwave irradiation. Especially, Fig. 2d and Fig. S3 show the growth of CNTs between the graphene sheets. During the additional microwave irradiation, CNTs grow by tailing the movement of the nickel nanoparticles. The direction of CNT growth was not necessarily unidirectional. Actually the nickel nanoparticles moved randomly, leading to the tip growth mechanism. Some CNTs were bent or curled, as shown in Fig. 2e. Moreover, it was possible to induce these CNTs to grow to a few micrometers in length by controlling the radiation time. Fig. 2f shows that the growth of CNTs is uniform on the graphene sheets and that there is a well-packed forest of CNTs. These CNTs are densely on the inner and outer surfaces of graphene.

The TEM image shown in Fig. 3 confirms the formation of the 3D G-CNT-Ni nanostructures. Fig. 3a shows well grown CNTs of various sizes of up to several nanometers in length.

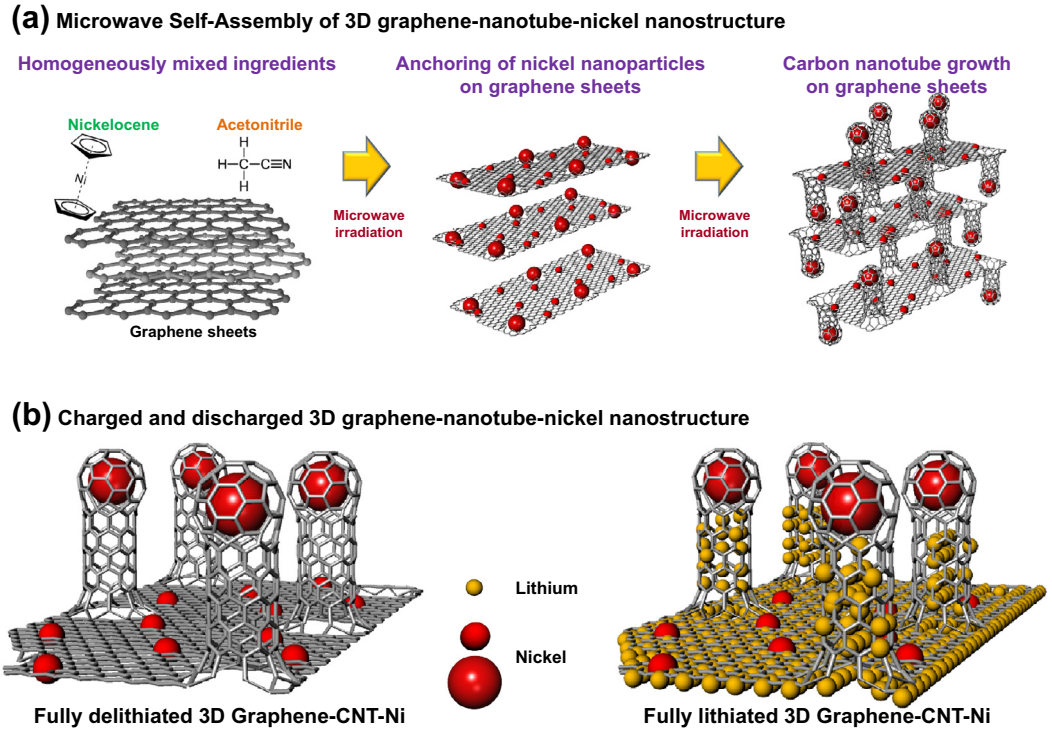

Fig. 1 – Schematics of (a) microwave-assisted synthesis of self-assembled 3D G-CNT-Ni nanostructure, and (b) 3D G-CNT-Ni nanostructure as an anode material during the charging and discharging processes in LIBs.

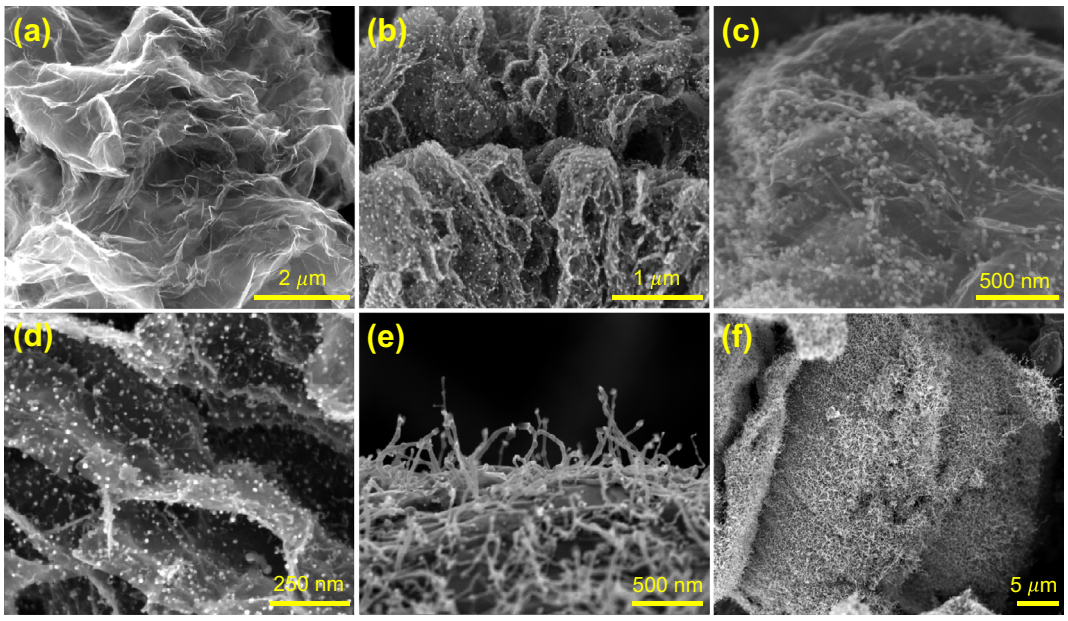

Fig. 2 – SEM images of (a) a wavy reduced graphene oxide sheet obtained by thermal exfoliation, (b) uniformly decorated nickel nanoparticles on the graphene sheets, (c) initiation of CNT growth by nickel nanoparticles from the graphene surface, (d) well distributed nickel nanoparticles on the inner and outer surfaces of graphene, which induce CNT growth between graphene layers, (e) full-grown CNTs after completion of the microwave irradiation, and (f) CNTs densely grown over several graphene sheets, showing self-assembled 3D G-CNTs-Ni nanostructures.

CNTs of various lengths and diameters are attached to the graphene sheets. The diameter of the CNTs strongly depends on the particle size of nickel [23]. Through a deep investigation of the 3D G-CNT-Ni nanostructures, we found that most nickel nanoparticles are observed inside the CNTs. That is, nickel nanoparticles remained in the CNTs after finishing the growth of CNTs. Fig. 3b shows the bamboo-shaped nature of the as-grown CNTs. These CNTs assume a bamboo-shaped structure due to the incorporation of nitrogen defects. Fig. 3c,d show the energy dispersive spectrometer (EDS) mapping of unique CNTs including nickel nanoparticles. Fig. 3c reveals the carbon maps of high angle annular dark field-scanning transmission electron microscopy (HAADF-STEM) image for bamboo-shaped CNTs. However, the carbon mapping is not clear due to the use of holey-carbon-film as a substrate. Ni elements are expressed as yellow parts in the EDS mapping, as shown in Fig. 3d. Typically, these encapsulated nickel particles corresponded to the XRD results shown in Fig. 4a.

XRD was used to confirm the phases of the starting material and the final product of the 3D G-CNT-Ni nanostructure. The XRD patterns of the TErGO and 3D G-CNT-Ni nanostructures are shown in Fig. 4a. A typical 2θ peak in graphene corresponding to the (002) diffraction peak was observed at 25.2° in the XRD pattern of TErGO. The d-spacing value was about 0.35 nm. This value is slightly larger than the peak of graphite (0.336 nm), suggesting that TErGO has some atomic scale defects in the basal planes and residual oxygen-functional groups [26]. In the 3D G-CNT-Ni nanostructures, this peak slightly shifted to 26.2° in the XRD pattern. During the formation of 3D G-CNT-Ni nanostructures, the residual oxygen-functional groups were removed, leading to a decrease in the d-spacing value to 0.33 nm. Besides this, in the XRD pattern of 3D G-CNT-Ni, as shown in Fig. 4a, new peaks at 44.42, 51.76, and 76.26°, corresponding to (111), (200), and (220) peaks from nickel nanoparticles are also observed [27]. This indicates that the nickel catalyst remained as nickel nanoparticles in the 3D G-CNT-Ni nanostructures [28]. Especially, the nickel particles encapsulated with carbon layers show pure peaks of nickel rather than that of nickel oxide (NiO) [27,28].

FT-IR study in the range of 4000–400 cm^{-1} was carried out in the present study. The FT-IR spectra of the TErGO and 3D G-CNT-Ni nanostructures are presented in Fig. 4b. In the TErGO and 3D G-CNT-Ni nanostructures, the peaks at 3400 cm^{-1} in the IR spectrum are attributed to O-H stretching. In the spectra acquired from the TErGO, the peak at 1739 cm^{-1} and the broad peak region near 1160 cm^{-1} correspond to residual carboxyl groups and epoxy functional groups after the thermal exfoliation, respectively [29]. In the spectra acquired from the 3D G-CNT-Ni nanostructures, such broad peaks (1160 cm^{-1}) in the identical regions are so altered, as shown in Fig. 4b. In this region, some oxygen-containing functional groups were partially shifted and split into two groups at 1200 and 1005 cm^{-1} after microwave irradiation. During the microwave irradiation, some oxygen-functional groups were removed by heat energy and some defects were formed on the surface of graphene. These defects acted as nucleation sites, at which nickel nanoparticles were anchored and gave rise to CNTs [22]. From this, atomic binding occurred between CNTs and graphene, resulting in the construction of the 3D G-CNT-Ni nanostructures. The peaks at 1550 and 1535 cm^{-1} in both materials correspond to the skeletal vibration of

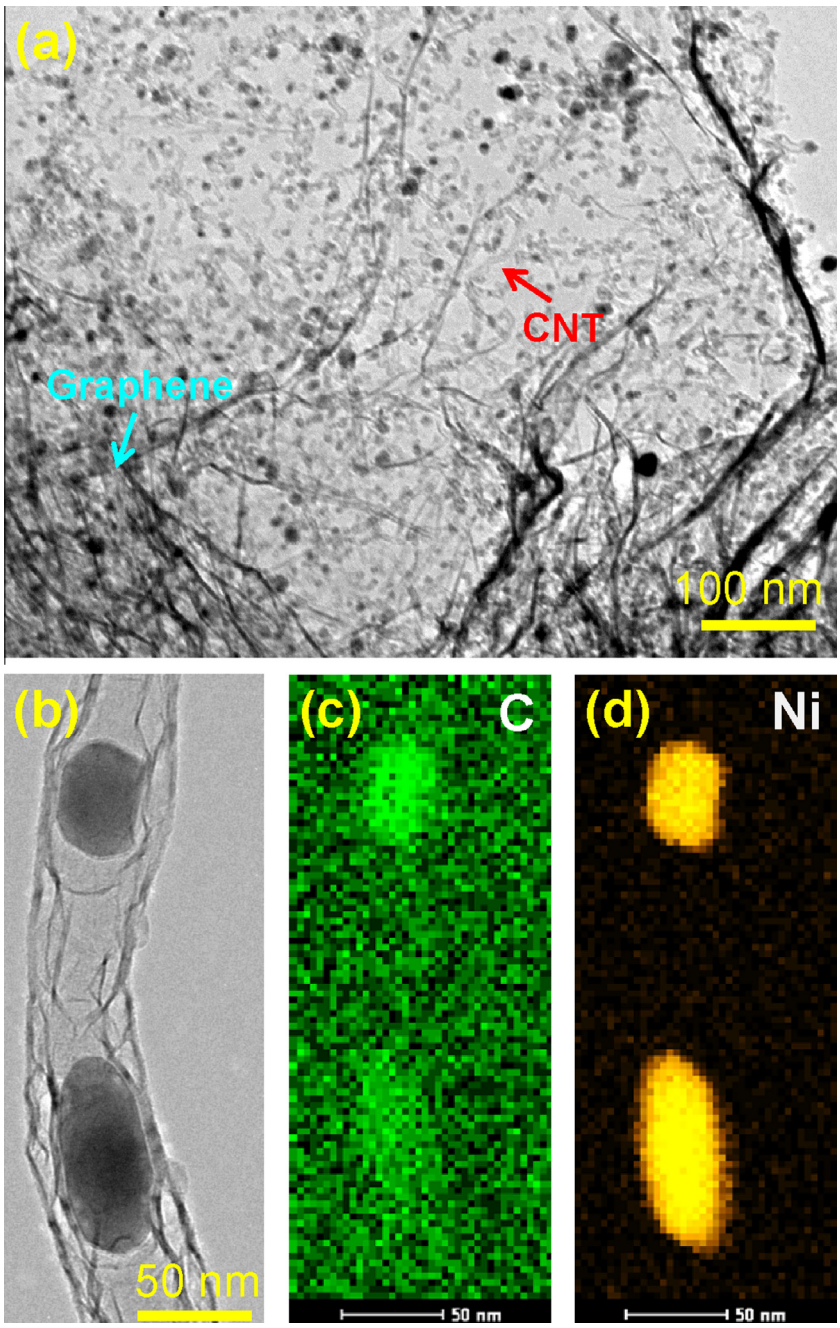

Fig. 3 – TEM images of (a) curled CNTs on wrinkled paper-like graphene sheets, (b) nickel nanoparticles inside bamboo-shaped CNTs and EDS maps of HAADF-STEM image for (c) carbon, and (d) nickel atoms in 3D G-CNT-Ni nanostructures.

graphene [16,30], which indicates that graphene existed in the material before and after the reactions.

It is well known that Raman spectroscopy, as a non-destructive technique, plays a critical role in characterizing 3D graphene-based materials. Therefore, this tool has been employed to obtain information about new structures and defects in this study. Fig. 4c shows Raman spectra acquired from the TErGO and 3D G-CNT-Ni nanostructures. There are two prominent bands in the spectra of each sample. The TErGO used as the starting material exhibited D and G bands at 1346 and 1571 cm^{-1}, respectively. However, the 3D G-CNT-Ni nanostructures exhibited D and G bands at 1352 and 1577 cm^{-1}, respectively. A small shift of 6 cm^{-1} toward the lower wavenumber side of the G band is observed compared to that the G band in the spectra of the TErGO. The shift of the G band in the 3D G-CNT-Ni nanostructures is related to the charge transfer between carbon material and the other compounds [31–33]. Therefore, the shift indicates that the 3D G-CNT-Ni nanostructures are produced in the form of a composite with direct bonding after microwave irradiation and that charge transfer occurs among the graphene sheets, nickel nanoparticles, and CNTs. The intensity ratio of the D–G band (I_D/I_G) of the 3D G-CNT-Ni nanostructures is 0.71, while that of the TErGO is 0.58. In Raman spectroscopy, the

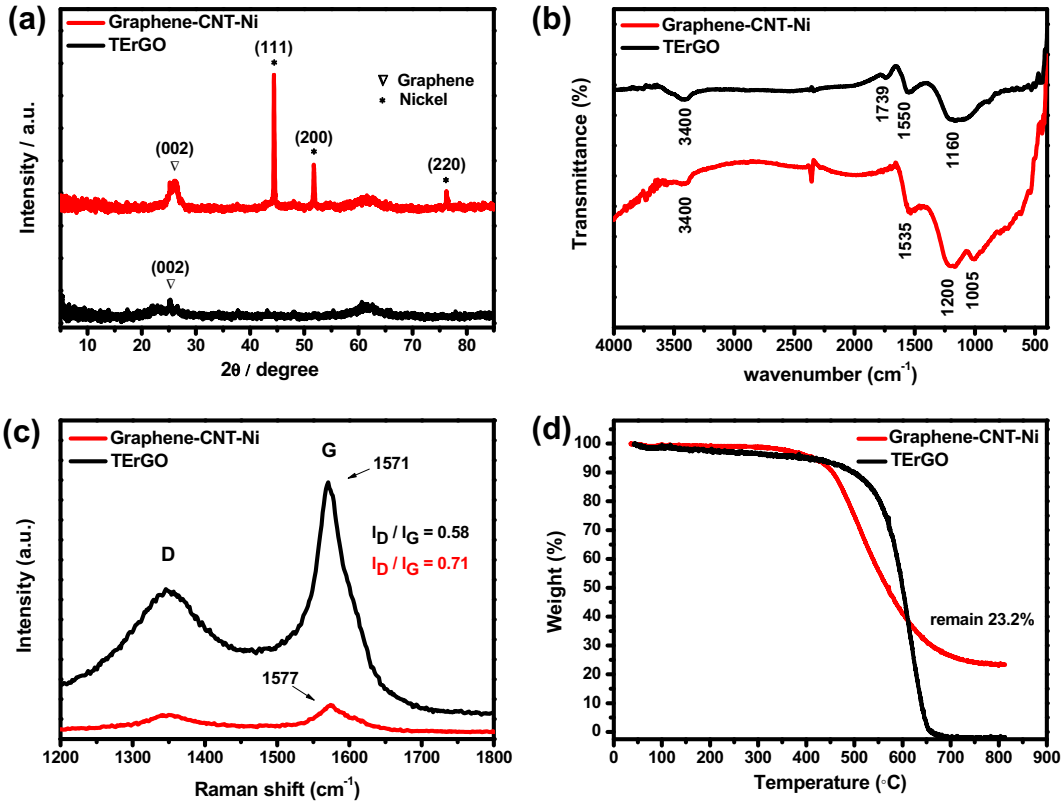

Fig. 4 – (a) XRD patterns, (b) FTIR spectra, (c) Raman spectra, and (d) TGA curve of TErGO and 3D G-CNT-Ni nanostructures.

D band indicates the extent of disorder in the crystalloid. Thus, a slight increase in I_D/I_G means an increase in disorder. It was arising from the remaining nickel nanoparticles inside of CNTs, and that CNTs which are present between (or intercalated into) the graphene sheets [32,34]. This result reveals that the levels of disorder in the basal planes of 3D G-CNT-Ni nanostructures are higher than that of TErGO.

The weight percentage of nickel in the 3D G-CNT-Ni nanostructure has been confirmed by TGA as shown in Fig. 4d. When comparing the both TGA curves, the TErGO curve shows a sharp decrease in weight at temperatures over 500 °C. Since TErGO is mainly composed of carbon and oxygen functional groups, all carbon material burns out in air or causes the formation of carbon dioxide until 800 °C. However, the weight of the 3D G-CNT-Ni nanostructures also decreases from around 500 °C: 23.2 percent of the material was left after 800 °C. That means that the nickel composition is nearly 23.2%, including both nickel catalysts and residual nickel in the 3D G-CNT-Ni nanostructures.

In order to investigate the change in the internal bonding of the structure after microwave irradiation, XPS analysis was conducted for the two materials. In Fig. 5a, the C 1s spectra of TErGO is shown to possess three peaks at 284.6, 286.2, and 290.6 eV, corresponding to sp^2 carbon, hydroxyl groups, and carboxyl groups, respectively [35]. The higher intensity of the non-oxygenated peak, located at 284.6 eV, indicates the completion of the thermal reduction process. After microwave irradiation, only very small residual oxygen functional groups still remained, as shown in Fig. 5c. However, there were some major changes in bonding between the oxygen groups. Before comparing the O 1s spectra of the TErGO with that of the 3D G-CNT-Ni nanostructures, the relative intensity ratio of oxygen can be seen to have dropped from 11.74% to 3.41% (Table S2). Inside the envelope, there was an extra low intensity peak at 529.7 eV in the 3D G-CNT-Ni nanostructure. This new binding state of oxygen suggests that the residual nickel nanoparticles, which were not used in CNT growth as catalysts, might have bonded to oxygen and led to the formation of NiO [36].

This can also be confirmed by surveying the nickel spectra. In the Ni 2p spectra (Fig. S1), the overall curve shapes correspond to the NiO spectra [33]. However, the noise level of the low intensity peaks appears to be due to the powder-type samples. Moreover, only a tiny content of nickel contributed to form the NiO (Table S2). In short, most of the nickel in the 3D G-CNT-Ni exists as nickel nanoparticles encapsulated inside CNTs, as shown in Fig. 3b; a small amount of the nickel is in the state of NiO.

To estimate the possibility and the potential synergy effects of using 3D G-CNT-Ni anode material for LIBs, an electrochemical test of the 3D G-CNT-Ni electrode was conducted. Besides, the results were compared with those for the bamboo-shaped CNT (CNT-Ni) electrode. Fig. 6a presents the first charge/discharge profiles of the 3D G-CNT-Ni nanostructure and the bamboo-shaped CNT electrodes at a current density of 100 mA/g. At the early stages of discharge curve, the profile of the bamboo-shaped CNTs decreases steeply from 3.0 to 1.0 V, while the profile of the 3D G-CNT-Ni nanostructure electrode decreased to 1.7 V. The capacity differences of lithium accommodation are mainly based on the

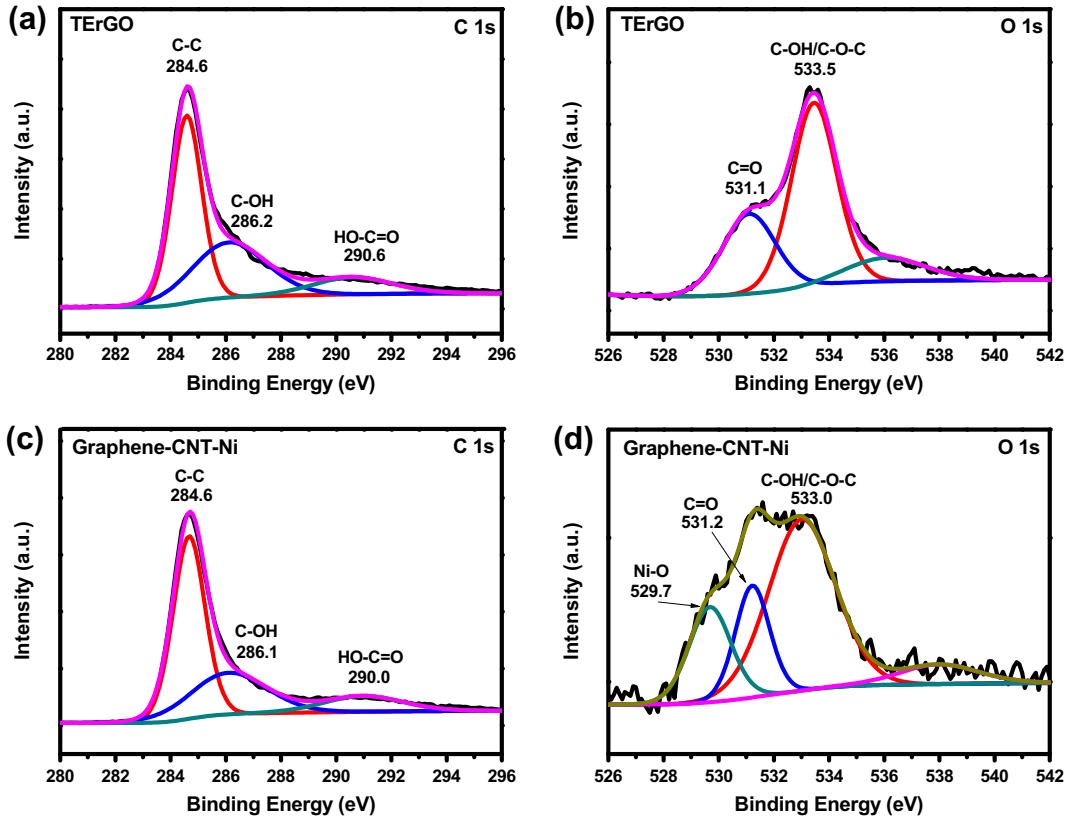

Fig. 5 – XPS analysis corresponding to (a) C 1s and (b) O 1s peaks of TErGO and (c) C 1s and (d) O 1s peaks of the 3D G-CNT-Ni nanostructures.

specific surface area (Table S1), resulting in a severe reduction of the specific capacity of about 200–300 mA h/g. In the initial discharge, a long distinct plateau was observed at 0.75 V and at 1 V for the bamboo-shaped CNTs and the 3D G-CNT-Ni nanostructure electrode, respectively. The formation of this plateau is due to the conversion reaction between nickel and Li. In addition, both the electrodes exhibited another pleateau below 0.5 V, which corresponds to the interaction between the composite materials and the electrolyte, forming a solid electrolyte interface (SEI) layer [37].

It can be seen in Fig. 6a that initial capacites of 1088.6 and 2395.2 mA h/g were obtained from the Li/bamboo-shaped CNTs and the Li/3D G-CNT-Ni half cells, respectively. It is apparent that the initial discharge capacity values for both the composite electrodes were greater than the expected theoretical capacities. This excess capacity of the electrodes arose from (1) decomposition of the electrolyte at a lower potential subsequent to the formation of SEI on the surface of the electrode, (2) reduction of the adsorbed impurities on the active material surfaces and (3) the reversible formation and decomposition of lithium oxide, as well as possible interfacial lithium ion storage.

As shown in Fig. 6a, the 3D G-CNT-Ni electrode showed lithium storage behavior better than that of the bamboo-shaped CNT electrode. The improved performance of the 3D G-CNT-Ni electrode is mainly attributed to the addition of a graphene matrix, resulting in the improvement of the electrical conductivity and an increased surface area. Therefore, the 3D G-CNT-Ni nanostructures can provide more reaction sites for redox cycling. Moreover, the structures lead to a smaller diameter of active particles, which induces a shorter diffusion length for Li-ions, enhancing the reaction kinetics and, thereby improving the overall electrochemical performance of the 3D G-CNT-Ni nanostructure electrode. Furthermore, the addition of the graphene matrix not only increases the electrical conductivity of the composite, but also facilitates more electrolyte adsorption through the open network system formed during the microwave irradiation, as shown in the SEM images in Fig. 2; this 3D network system stabilizes the electrode–electrolyte interface and hence improves the storage capabilities in an exceptional way. In contrast, the bamboo-shaped CNT electrode delivered relatively low capacity compared to that of the 3D G-CNT-Ni composite due to the agglomeration of CNTs during the preparation, which affects the connectivity between the nanotube network and the Ni particles, thus limiting the lithium ion storage property of the bamboo-shaped CNT composite [38]. Although the 3D G-CNT-Ni electrode delivered capacity higher than that of the other electrodes, it also has a large irreversible capacity loss (ICL). This large ICL could be attributed to the presence of oxygen functional groups in the 3D G-CNT-Ni composite, as is evident in the XPS studies, as shown in Fig. 5. These functional groups in the composite can irreversibly entrap Li^+ions and thereby lead to large ICL [39]. It is in under progress to reduce the irreversible capacity during the initial cycle by controlling the specific surface area and optimizing the electrolyte with additives

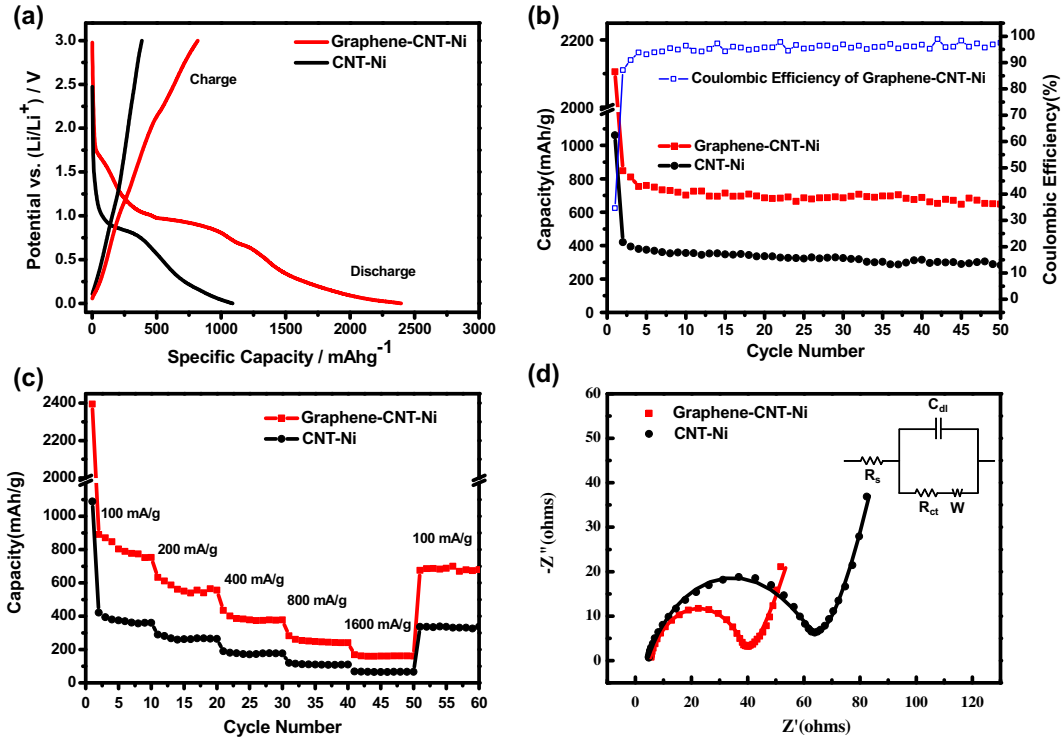

Fig. 6 – (a) First charge/discharge profiles of 3D G-CNT-Ni nanostructures and bamboo-shaped CNTs between 0 and 3.0 V at a current density of 100 mA/g. (b) Cyclic performance of 3D G-CNT-Ni nanostructures and bamboo-shaped CNTs up to 50 cycles at a current density of 100 mA/g. (c) Rate performance of 3D G-CNT-Ni nanostructures and bamboo-shaped CNTs. (d) Nyquist plots of 3D G-CNT-Ni nanostructures and bamboo-shaped CNTs. Symbols, experimental data; lines, fitted data. Inset and insert shows the equivalent circuit.

because the large irreversible capacity loss is not favorable for LIBs in commercial applications.

In order to compare the effect of graphene addtion on the cycliability, cycle tests of these two materials were conducted at 100 mA/g between 0 and 3.0 V, with results as shown in Fig. 6b. The 3D G-CNT-Ni nanostructure maintains a very high reversible specific capacitiy of 648.2 mA h/g after 50 cylces. However, the reversible capacity of the bamboo-shaped CNT electrode was about 282.4 mA h/g. The value is much smaller value than the reversible capapcity of the 3D G-CNT-Ni nanostructure electrode. This remarkable difference in the cycle performance between the two materials could be the result of the unique structural characteristics of the 3D G-CNT-Ni electrode. Since the 3D G-CNT-Ni nanostructure had high surface-to-volume ratio, this 3D structure possesses high stability during the charge and discharge process; this high stability results from the good mechanical flexibility of graphene, which contributes to the reduction of the large volume change. Moreover, CNTs grown between the graphene layers acted as spacers. Therefore, the 3D nanostructure mitigates self-aggregation and re-stacking of the graphene layers and provides more available active sites for the electrochemical reaction. Moreover, the interactions of the graphene, due to its high van der Waals force, formed an open network system, through which electrolyte species were easily able to access the surface of the graphene layer, improving the formantion of SEI. This process also increased the utilization of electrode active species during the electrochemical reaction process. It is noteworthy that the hybridization of CNTs and ultrathin graphene sheets leads to the formation of a highly conductive 3D graphene network with highly porous morphology, as illustrated in Fig. 2. This conductive 3D network significantly improved the overall conductivity of the composite electrode and the carrier mobility, thereby ensuring excellent cycling performance [38].

The rate performances of the 3D G-CNT-Ni nanostructure and of the bamboo-shaped CNT electrodes are shown in Fig. 6c. The rate performance measurement was conducted at the specific current densities of 100, 200, 400, 800, and 1600 mA/g between the potential range of 0 and 3.0 V. It can be seen from Fig. 6c that the discharge capacity of both electrodes was gradually decreased with increasing current density. This is due to the polarization effect of the electrodes at high current rates, which reduces the time required for Li-ion diffusion. Hence, Li-ion can participate mainly on the surface of the electrode materials in the high rate charging-discharging process. It should be noted in Fig. 6c that the cell containing the 3D G-CNT-Ni nanostructure electrode showed much higher specific capacitiy than that of the bamboo-shaped CNT electrode at all current densities. After returning to 100 mA/g, the 3D G-CNT-Ni nanostructure electrode still showed a high specific capacity value of 699 mA h/g, even after being cycled at high current rates; this specific capacity value is higher than that in previous reports and is also comparable with values of other 3D carbon/carbon composites [3,7,16,25]. These results provide strong evidence that the

electrochemical process of the 3D G-CNT-Ni nanostructure electrode is highly reversible to a certain extent. It is possible to explain the excellent rate performance of the 3D G-CNT-Ni nanostructure electrode, resulting from the enhanced electrochemical reactivity. It is due to the large specific surface area of 3D G-CNT-Ni nanostructures and the nano-crystalline nature of nickel particles. Hence, this improved electrochemical performance was realized for the 3D G-CNT-Ni nanostructure electrode even at the high current rates. Although the bamboo-shaped CNT electrode showed electrochemical activity, the agglomeration of CNTs during the irradiation, due to the van der Waals force, reduced the flexible nature of the nanotubes, as well as the surface area of the composite, thus affecting the protection of the SEI layer at high current rates and hence decreasing the lithium storage capacity [38].

Several EIS studies were consulted to determine the influence of graphene addition on the electrical conductivity; the corresponding Nyquist plots are presented in Fig. 6d. The Nyquist traces were fitted according to an equivalent circuit (inset in Fig. 6d); the fitting parameters are listed in Table S3. The Nyquist plots of the 3D G-CNT-Ni nanostructure and of the bamboo-shaped CNT electrodes are similar; both showed a semi-circle in the low frequency region and an inclined line in the high frequency region. The semi-circle at low frequency region represents the resistance associated with the charge transfer resistance (Rct), which is used to measure the electrochemical reaction kinetics. On the other hand, the sharp upward line in the high frequency region corresponds to Li-ion diffusion into the bulk of the electrode. According to the fitting data shown in Table S3, the Rct values of the bamboo-shaped CNT and the 3D G-CNT-Ni nanostructure electrodes were calculated and found to be about 60.11 and 34.50 Ω, respectively. It is clear that the cell containing the 3D G-CNT-Ni nanostructure electrode has a lower R_{ct}, demonstrating that the addition of graphene has effectively reduced the cell resistance. It is a noteworthy fact that the lowering of the resistance directly increases the current access on the electrode, enhances the Li-ion diffusion rate toward the electrode, and improves the electrochemical reactivity of the 3D G-CNT-Ni nanostructure electrode. The EIS results correlate well with the charge and discharge studies.

4. Conclusions

We have developed a microwave-assisted method to synthesize self-assembled 3D G-CNT-Ni nanostructures for use as high-capacity anode materials in LIBs. Microwave-assisted thermal heating delivers a huge amount of energy in a short duration, leading to fast chemical decomposition and reactions, finally forming a self-assembled 3D carbon nanostructure. CNTs are vertically grown on the graphene sheets through the tip growth mechanism by Ni nanoparticles. The CNTs firmly standing on the graphene sheets play the role of spacers, preventing graphene layers from re-stacking and self-agglomerating. Moreover, the 3D G-CNT-Ni nanostructures electrode shows enhanced reversible performances in cyclic and rate tests, maintaining the specific capacity of 648.2 mA h/g after 50 cycles at a current density of 100 mA/g. These unique 3D G-CNT-Ni nanostructures have the potential for use in backbone structures of anode materials in LIBs.

Acknowledgments

This work was supported by the International Cooperation of the Korea Institute of Energy Technology Evaluation and Planning (KETEP) Grant funded by the Korea government Ministry of Knowledge Economy (No. 20128510010050). This research was supported by KAIST Institute for the NanoCentury.

Appendix A. Supplementary data

Supplementary data associated with this article can be found, in the online version, at http://dx.doi.org/10.1016/j.carbon.2013.08.003.

REFERENCES

[1] Wang G, Shen X, Yao J, Park J. Graphene nanosheets for enhanced lithium storage in lithium ion batteries. Carbon 2009;47(8):2049–53.
[2] Kokai F, Sorin R, Chigusa H, Hanai K, Koshio A, Ishihara M, et al. Ultrasonication fabrication of high quality multilayer graphene flakes and their characterization as anodes for lithium ion batteries. Diam Relat Mater 2012;29:63–8.
[3] Lee S-H, Seo S-D, Park K-S, Shim H-W, Kim D-W. Synthesis of graphene nanosheets by the electrolytic exfoliation of graphite and their direct assembly for lithium ion battery anodes. Mater Chem Phys 2012;135(2–3):309–16.
[4] Zou Y, Kan J, Wang Y. Fe_2O_3-graphene rice-on-sheet nanocomposite for high and fast lithium ion storage. J Phys Chem C 2011;115(42):20747–53.
[5] Yang S, Cui G, Pang S, Cao Q, Kolb U, Feng X, et al. Fabrication of cobalt and cobalt oxide/graphene composites: towards high-performance anode materials for lithium ion batteries. ChemSusChem 2010;3(2):236–9.
[6] Yoo E, Kim J, Hosono E, Zhou H-s, Kudo T, Honma I. Large reversible li storage of graphene nanosheet families for use in rechargeable lithium ion batteries. Nano Lett 2008;8(8):2277–82.
[7] Zhang LL, Zhao XS. Carbon-based materials as supercapacitor electrodes. Chem Soc Rev 2009;38(9):2520–31.
[8] Kabbour H, Baumann TF, Satcher JH, Saulnier A, Ahn CC. Toward new candidates for hydrogen storage: high-surface-area carbon aerogels. Chem Mater 2006;18(26):6085–7.
[9] Fan Z, Yan J, Zhi L, Zhang Q, Wei T, Feng J, et al. A three-dimensional carbon nanotube/graphene sandwich and its application as electrode in supercapacitors. Adv Mater 2010;22(33):3723–8.
[10] Kim Y-S, Kumar K, Fisher FT, Yang E-H. Out-of-plane growth of CNTs on graphene for supercapacitor applications. Nanotechnology 2012;23(1):015301.
[11] Brownson DAC, Banks CE. The electrochemistry of CVD graphene: progress and prospects. Phys Chem Chem Phys 2012;14(23):8264–81.
[12] Fan Z-J, Yan J, Wei T, Ning G-Q, Zhi L-J, Liu J-C, et al. Nanographene-constructed carbon nanofibers grown on graphene sheets by chemical vapor deposition: high-performance anode materials for lithium ion batteries. ACS Nano 2011;5(4):2787–94.
[13] Lee DH, Kim JE, Han TH, Hwang JW, Jeon S, Choi S-Y, et al. Versatile carbon hybrid films composed of vertical carbon nanotubes grown on mechanically compliant graphene films. Adv Mater 2010;22(11):1247–52.
[14] Tung VC, Chen L-M, Allen MJ, Wassei JK, Nelson K, Kaner RB, et al. Low-temperature solution processing of graphene-

carbon nanotube hybrid materials for high-performance transparent conductors. Nano Lett 2009;9(5):1949–55.
[15] Chen S, Chen P, Wang Y. Carbon nanotubes grown in situ on graphene nanosheets as superior anodes for li-ion batteries. Nanoscale 2011;3(10):4323–9.
[16] Chen T, Pan L, Yu K, Sun Z. Microwave-assisted synthesis of reduced graphene oxide–carbon nanotube composites as negative electrode materials for lithium ion batteries. Solid State Ionics 2012;229:9–13.
[17] Chen T, Pan L, Liu X, Yu K, Sun Z. One-step synthesis of SnO_2-reduced graphene oxide-carbon nanotube composites via microwave assistance for lithium ion batteries. RSC Adv 2012;2(31):11719–24.
[18] Zhu Y, Li L, Zhang C, Casillas G, Sun Z, Yan Z, et al. A seamless three-dimensional carbon nanotube graphene hybrid material. Nat Commun 2012;3:1225.
[19] Yan Z, Ma L, Zhu Y, Lahiri I, Hahm M-G, Liu Z, et al. Three-dimensional metal-graphene-nanotube multifunctional hybrid materials. ACS Nano 2012;7(1):58–64.
[20] Lee S-H, Sridhar V, Jung J-H, Kaliyappan K, Lee Y-S, Mukherjee R, et al. Graphene-nanotube-iron hierarchical nanostructure as lithium ion battery anode. ACS Nano 2013;7(5):4242–51.
[21] Hummers WS, Offeman RE. Preparation of graphitic oxide. J Am Chem Soc 1958;80(6):1339.
[22] Sridhar V, Kim H-J, Jung J-H, Lee C, Park S, Oh I-K. Defect-engineered three-dimensional graphene–nanotube–palladium nanostructures with ultrahigh capacitance. ACS Nano 2012;6(12):10562–70.
[23] Pham-Huu C, Vieira R, Louis B, Carvalho A, Amadou J, Dintzer T, et al. About the octopus-like growth mechanism of carbon nanofibers over graphite supported nickel catalyst. J Catal 2006;240(2):194–202.
[24] Mai YJ, Tu JP, Gu CD, Wang XL. Graphene anchored with nickel nanoparticles as a high-performance anode material for lithium ion batteries. J Power Sources 2012;209:1–6.
[25] Jeong N, Lee J. Growth of filamentous carbon by decomposition of ethanol on nickel foam: influence of synthesis conditions and catalytic nanoparticles on growth yield and mechanism. J Catal 2008;260(2):217–26.
[26] Wang C, Li D, Too CO, Wallace GG. Electrochemical properties of graphene paper electrodes used in lithium batteries. Chem Mater 2009;21(13):2604–6.
[27] Ko S, Takahashi Y, Sakoda A, Sakai Y, Komori K. Direct Synthesis of cup-stacked carbon nanofiber microspheres by the catalytic pyrolysis of poly(ethylene glycol). Langmuir 2012;28(23):8760–6.
[28] Wirth CT, Hofmann S, Robertson J. State of the catalyst during carbon nanotube growth. Diam Relat Mater 2009;18(5–8):940–5.
[29] Pan D, Wang S, Zhao B, Wu M, Zhang H, Wang Y, et al. Li storage properties of disordered graphene nanosheets. Chem Mater 2009;21(14):3136–42.
[30] Nethravathi C, Rajamathi M. Chemically modified graphene sheets produced by the solvothermal reduction of colloidal dispersions of graphite oxide. Carbon 2008;46(14):1994–8.
[31] Rao AM, Eklund PC, Bandow S, Thess A, Smalley RE. Evidence for charge transfer in doped carbon nanotube bundles from Ramen scattering. Nature 1997;388(6639):257–9.
[32] Zhou J, Song H, Ma L, Chen X. Magnetite/graphene nanosheet composites: interfacial interaction and its impact on the durable high-rate performance in lithium-ion batteries. RSC Adv 2011;1(5):782–91.
[33] Zhou G, Wang D-W, Yin L-C, Li N, Li F, Cheng H-M. Oxygen Bridges between nio nanosheets and graphene for improvement of lithium storage. ACS Nano 2012;6(4):3214–23.
[34] Kottegoda IRM, Idris NH, Lu L, Wang J-Z, Liu H-K. Synthesis and characterization of graphene–nickel oxide nanostructures for fast charge–discharge application. Electrochim Acta 2011;56(16):5815–22.
[35] Varghese B, Reddy MV, Yanwu Z, Lit CS, Hoong TC, Subba Rao GV, et al. Fabrication of nio nanowall electrodes for high performance lithium ion battery. Chem Mater 2008;20(10):3360–7.
[36] Wen B, Zhang S, Fang H, Liu W, Du Z. Electrochemically dispersed nickel oxide nanoparticles on multi-walled carbon nanotubes. Mater Chem Phys 2011;131(1–2):8–11.
[37] Wang XX, Wang JN, Su LF. Preparation and electrochemical performance of ultra-short carbon nanotubes. J Power Sources 2009;186(1):194–200.
[38] Saito R, Dresselhaus G, Dresselhaus MS. Physical properties of carbon nanotube. London: Imperial College Press; 1998.
[39] Bhaskar A, Deepa M, Rao TN, Varadaraju UV. Enhanced nanoscale conduction capability of a MoO_2/graphene composite for high performance anodes in lithium ion batteries. J Power Sources 2012;216:169–78.